European Journal of Radiology 84 (2015) 450–457

Contents lists available at ScienceDirect

European Journal of Radiology

journal homepage: www.elsevier.com/locate/ejrad

Evaluation of MR issues for the latest standard brands of orthopedic metal implants: Plates and screws

Yue-fen Zou[a,*], Bin Chu[a,1,4], Chuan-bing Wang[a,2,4], Zhi-yi Hu[b,3]

[a] Department of Radiology, The First Affiliated Hospital of Nanjing Medical University, No. 300 Guangzhou Road, Nanjing, China
[b] Department of Spine Surgery, The First Affiliated Hospital of Nanjing Medical University, No. 300 Guangzhou Road, Nanjing, China

ARTICLE INFO

Article history:
Received 15 May 2014
Received in revised form 2 December 2014
Accepted 4 December 2014

Keywords:
Magnetic resonance imaging
Orthopedic implant
Titanium alloy
Stainless steel
Safety
Artifacts

ABSTRACT

Purpose: The study was performed to evaluate magnetic resonance (MR) issues for the latest standard brands of plates and screws used in orthopedic surgery at a 1.5-T MR system, including the safety and metallic artifacts.

Methods: The plates and screws (made of titanium alloy and stainless steel materials, according to the latest standard brands) were assessed for displacement in degrees, MRI-related heating and artifacts at a 1.5-T MR system. The displacement in degrees of the plates and screws was evaluated on an angel-measurement instrument at the entrance of the MR scanner. The MRI-related heating was assessed on a swine leg fixed with a plate by using a "worst-case" pulse sequence. A rectangular water phantom was designed to evaluate metallic artifacts of a screw on different sequences (T1/T2-weighted FSE, STIR, T2-FSE fat saturation, GRE, DWI) and then artifacts were evaluated on T2-weighted FSE sequence by modifying the scanning parameters including field of view (FOV), echo train length (ETL) and bandwidth to identify the influence of parameters on metallic artifacts. 15 volunteers with internal vertebral fixation (titanium alloy materials) were scanned with MR using axial and sagittal T2-FSE, sagittal T2-FSE fat suppression and STIR with conventional and optimized parameters, respectively. Then all images were graded by two experienced radiologists having the experience of more than 7 years under double-blind studies that is neither of them knew which was conventional parameter group and optimized parameter group.

Results: The average deflection angle of titanium alloy and stainless steel implants were 4.3° and 7.7°, respectively, (less than 45°) which indicated that the magnetically induced force was less than the weight of the object. The deflection angle of the titanium alloy implants was less than the stainless steel one ($t = 9.69$, $P < 0.001$). The average temperature changes of titanium alloy before and after the scan was 0.48 °C and stainless steel implants was 0.74 °C, respectively, with the background temperature changes of 0.24 °C. The water phantom test indicated that the DWI sequence produced largest artifacts, while FSE pulse sequence produced smallest artifacts. And T2-weighted FSE fat saturation sequence produced larger artifacts than STIR sequence. The influence of the scanning parameters on metallic artifacts was verified that metallic artifacts increased with longer echo train length and bigger FOV, while decreased with larger bandwidth. The interreader agreement was good or excellent for each set of images graded with Cohen's Kappa statistic. Image grading of axial and sagittal T2-FSE with optimized parameters were significantly superior to that with conventional parameters (grade, 3.3 ± 0.5 vs 2.7 ± 0.6, $P = 0.003$; 3.2 ± 0.4 vs 1.9 ± 0.7, $P = 0.001$) and image of STIR sequence received a better grade than T2-FSE FS sequence (grade, 3.4 ± 0.5 vs 1.7 ± 0.6, $P < 0.001$).

Conclusions: The latest standard plates and screws used in orthopedic surgery do not pose an additional hazard or risk to patients undergoing MR imaging at 1.5-T or less. Though artifacts caused by them cannot be ignored because of their relatively large size, it is possible to be minimized by choosing appropriate pulse sequences and optimizing scanning parameters, such as FSE and STIR sequence with large bandwidth, small FOV and appropriate echo train length.

© 2014 Elsevier Ireland Ltd. All rights reserved.

* Corresponding author. Tel.: +86 13951606287; fax: +86 25 83780711.
E-mail addresses: zou_yf@163.com (Y.-f. Zou), 18262636700@163.com (B. Chu), wangchuanb_csr@163.com (C.-b. Wang), huzhiyi@medmail.com.cn (Z.-y. Hu).
[1] Tel: +86 18262636700.
[2] Tel: +86 13912985425.
[3] Tel: +86 13851657808.
[4] Both authors are co-first authors and contributed equally to the work.

http://dx.doi.org/10.1016/j.ejrad.2014.12.001
0720-048X/© 2014 Elsevier Ireland Ltd. All rights reserved.

1. Introduction

With the progression of orthopedic techniques and development of biological materials, metallic implants have been used widely, such as internal fixation of bone-fracture, spinal fusion, and artificial joint replacement. The number of follow-up patients with metallic implants is becoming larger and larger. Local complications of passive implants have been well recognized in previous study and include heterotopic bone formation, mechanical aseptic loosening of prosthesis, prosthetic or peri-prosthetic fracture, superficial and deep infections, foreign-body granulomatosis, and osteolysis [1–3]. Radiography is the initial imaging modality of choice for evaluating the post-operative implants. But its ability to display complications is limited to a larger extent. Computed tomography (CT) and magnetic resonance imaging (MRI) are more advanced modalities to assess passive implants and complications. Because of its superior soft tissue contrast and tomographic capabilities, MR imaging can better depict the extent and volume of osteolysis involvement compared to radiography and has been shown to be more sensitive and specific than optimized CT or plain radiographs in the detection of focal osteolytic lesions [4–6].

However, when a patient with metallic implants will undergo MRI, we have to consider two aspects: (1) the safety of patient (2) artifacts around the implants. Although previous studies have indicated that most of the orthopedic implants are compatible in MR imaging system especially for titanium alloy, there are still concerns about the safety of patients with stainless steel implants, who were refused to a MR scan in most cases in our country. To ensure the safety of patients with metallic implants, it is necessary to conduct in vitro test using standardized techniques to evaluate displacement force and MRI-related heating [7–9]. In addition, artifacts caused by metallic implants present problems if MR imaging area of interest is in or near passive implants. For a passive implant, it is well known that artifacts are dependent on the magnetic susceptibility of the materials, the object's dimensions, imaging pulse sequences, parameters and other factors [1,7,8]. Our study also was performed to evaluate the influence of different pulse sequences and parameters on artifact size to obtain optimized pulse sequences with appropriate parameters for reducing artifacts.

In considering the mentioned information above, the objective of our investigation was to assess MR issues (i.e., displacement in degrees, MRI-related heating, artifacts) for the latest standard brands of plates and screws used in orthopedic surgery at a 1.5-T MR system.

2. Materials and methods

2.1. Plates and screws

Plates and screws (Stryker, USA; Weigao Medical Polymer Co., Shandong, China; Zhengda Medical Care, Tianjin, China) for internal fixation of fracture were selected to evaluate MR issues. Parts of them were titanium alloy materials and the other were stainless steel materials, with length from 2.4 cm to 19.2 cm (Fig. 1). The titanium alloy materials are the most commonly used alloy at present in our country, known as Ti-6Al-4V, conforming to ISO5832-3 (International Organization for Standardization) and GB/T13810-2007 standards. The grade of stainless steel materials is OOCr18Ni14Mo3, conforming to ISO5832-1 and GB4234-2007 standards, which is also the most popular medical stainless steel implants in recent years.

Fig. 1. Plates and screws used for displacement force test: titanium alloy materials (left) and stainless steel materials (right).

2.2. Displacement in degrees

The total implants were 14 that includes 7 for the titanium alloy implants and the other 7 for stainless steel implants (Fig. 1). The displacement in degrees of the implants was assessed on an angel-measurement instrument designed by ourselves at the entrance of the MR scanner, where the largest force was produced, according to the recommended standards of the American Society for Testing and Materials (ASTM) [10] (Fig. 2). The plates and screws were suspended from a lightweight string (25-cm in length; weight, less than 1% of the weight of each implant) attached to the 0° indicator position on the protractor. The maximum deflection angle of each implant from the vertical direction was measured [7–11].

Fig. 2. An angel-measuring instrument which was self made: the plate was positioned in the area where the largest attraction force was produced.

Fig. 3. Plates used for MRI-related heating test: titanium alloy materials (left) and stainless steel materials (right).

According to the ASTM F2213-06 [12], the relationship of magnitude between the magnetically-induced force of object and its weight could indicate the safety of displacement force and torque, and the deflection angle of the implant was used in our test. But the torque considered here was the magneto-static torque due to the interaction of the MRI static magnetic field with the magnetization in the implant. The dynamic torque due to interaction of the static field with eddy currents induced in a rotating device was not addressed.

2.3. MRI-related heating

MRI-related heating at the 1.5-T MR system was evaluated for 10 plates with 5 of titanium alloy materials and 5 of stainless steel materials, which were implanted in a swine leg, respectively (Figs. 3 and 4). Relatively high level radiofrequency (RF) energy was applied during this experiment. All of the implants and the swine leg were placed into the MR examination room for more than 6 h to achieve balanced temperature. Two mercurial thermometers (Shanghai Medical Equipment Works Co., China) were used for recording temperature. The temperature was measured only at the mid portion of all the implants which were in contact with the bone and the other temperature was measured at mid portion of the other side of the bone parallel to the implant. To ensure that we have no temperature difference among all we measured the temperature at the same position for all the implants. Temperature of both thermometers was recorded immediately before and after each time of MR scanning [9,13,14].

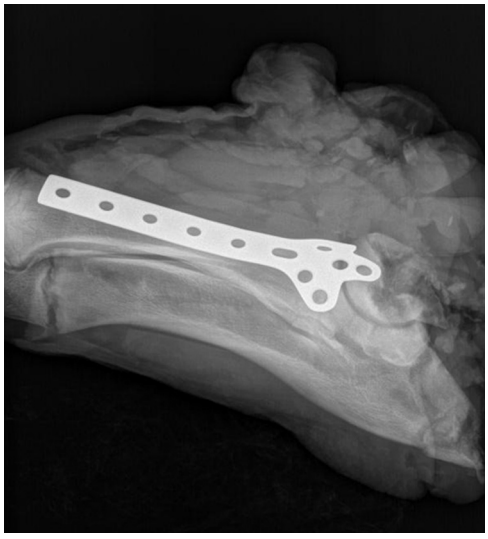

Fig. 4. Specimen for MRI-related heating test: a swine leg with plate implantation.

2.4. MRI conditions

MRI-related heating test was conducted at 1.5-T/64-MHz (Signa HDxt, GE Healthcare), using body coil to transmit and receive radiofrequency (RF) energy. MRI parameters were selected to generate a relatively high level of RF energy representing the "worst-case" in clinical condition. According to the standards of ASTM [14], fast spin echo (FSE) sequence was used with the parameters as follows: number of excitations (NEX) of 12, flip angle (FA) of 90°, repetition time (TR) 4500 ms, echo time (TE) 138 ms, a matrix of 320 × 224, bandwidth of 125 kHz, echo train length (ETL) of 49, the whole body average specific absorption rate (SAR) of 1.85-W/kg and scanning time of 15 min. The averaged SAR value was displayed on the system automatically when the MR sequence and parameters were determined and the maximal averaged SAR value was used to indicate the "worst-case" condition of the localized area. Because this experimental specimen was lack of "blood flow", it simulated an extreme condition to assess MRI-related heating for this implant [11,14,15].

2.5. Artifacts

A rectangular water phantom made of poly methyl methacrylate plastic with dimension of 27.2 cm × 13.5 cm × 17.4 cm (length, width, height) was designed to evaluate the metallic artifacts of a titanium alloy screw under different sequences. The water phantom was filled with copper sulfate ($CuSO_4$) solution (1 g/L) to reduce T1 and keep TR at a reasonable level. The screw (length 55 mm, diameter 15 mm) was immersed in the center of the solution fixed by three thin nylon threads. MR imaging was performed using the 1.5-T/64-MHz (Signa HDxt, GE Healthcare), a transmit/receive head RF coil and the following pulse sequences:T1/T2-weighted fast spin echo(FSE), short TI inversion recovery (STIR), T2-weighted FSE fat saturation (FS), gradient echo (GRE), diffusion-weighted imaging (DWI) [7,8,15,16], the parameters are shown in Table 1.

To identify the influence of MR scan parameters on size of metallic artifacts, T2-weighted FSE sequence and a titanium alloy screw were selected. The screw and water phantom as previously mentioned were used to achieve image artifacts by altering field of view (FOV), echo train length (ETL) and bandwidth, respectively, with other parameters keeping unchanged.

In all cases two sets of images (with and without the implant) were acquired to obtain images with and without artifacts. The images were obtained and analyzed according to the method from ASTM F2119-01 [17]. Planimetry software provided with Medavis PACS system was used to measure the size of artifacts. A rectangular region of interest (ROI) was drawn on the two sets of images (with and without implant) enclosing the visible artifacts. Window level and window width of the image with artifacts were determined from the same ROI position in the image without artifacts. Window center was set to the mean signal intensity within the ROI in the image without artifacts, and window width was set to a 60% of that window center. Then the maximal length and width of the artifacts (containing size of screw) were measured three times on the plane with the maximal artifacts (Fig. 5), each with an interval of one day [9,11,17].

According to the influence of parameters on artifacts size, the conventional sequence parameters were modified to achieve optimized pulse sequence for reducing artifacts. Then 15 volunteers with internal vertebral fixation (titanium alloy materials) were performed MR scan with conventional and optimized parameters, respectively. The pulse sequences of axial and sagittal T2-FSE, sagittal T2-FSE fat suppression and STIR were used. The parameters

Table 1
Sequence parameters for metal artifacts test.

Sequences	Bandwidth (kHz)	TR/TE (ms)	Flip angle degree (°)	Slice thick (mm)	FOV (cm)	Matrix
FSE-T1	31.25	1785/26	90	4	24 × 24	320 × 192
FSE-T2	31.25	4000/110	90	4	24 × 24	320 × 192
STIR	31.25	5000/55	90	4	24 × 24	320 × 192
FSE-T2-FS	31.25	4000/110	90	4	24 × 24	320 × 192
GRE	–	5.5/1.7	30	4	24 × 24	320 × 192
DWI	b = 1000	4500/80	90	4	24 × 24	320 × 192

Note. TR = repetition time, TE = echo time, FOV = field of view.

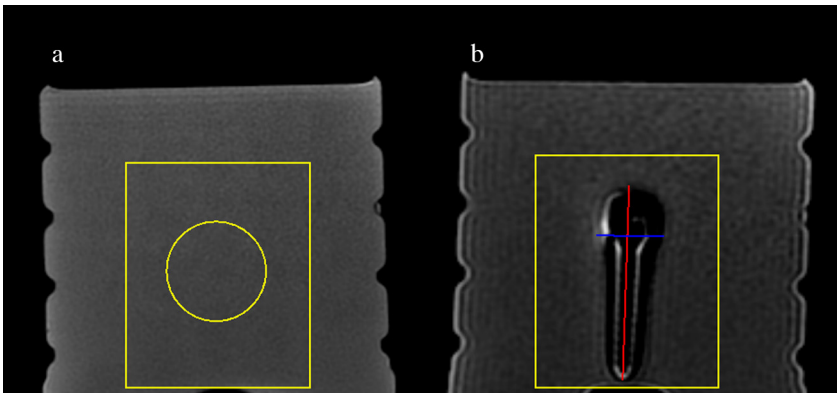

Fig. 5. A set of images for the artifact measurement: (a) the image with copper sulfate solution (without screw) and (b) the image with screw. The rectangle box represented the ROI containing the visible artifacts. The circle was used to measure the mean signal intensity of the ROI without artifacts, which was set as the window center for (b). And the window width of (b) was set to a 60% of that window center. Then the artifacts on (b) were relatively obvious. Red and blue lines on (b) represent the maximal length and width of the artifacts, respectively. These steps were done three times to acquire one set of images and the mean value was obtained. (For interpretation of the references to color in this figure legend, the reader is referred to the web version of this article.)

Table 2
Conventional (CO) and optimized (OP) sequence parameters.

Sequences	Bandwidth (kHz)	TR/TE (ms)	Flip angle degree (°)	Slice thick (mm)	FOV (cm)	Matrix	ETL
CO-sagittal-FSE-T2	41.67	3140/102	90	4	32 × 32	384 × 160	21
CO-axial-FSE-T2	27.78	3200/120	90	4	20 × 20	320 × 192	19
CO-sagittal-FSE-FS	31.25	2680/102	90	4	32 × 32	320 × 224	21
OP-sagittal-FSE-T2	142.86	1600/102	90	4	32 × 32	384 × 256	15
OP-axial-FSE-T2	142.86	2020/120	90	4	20 × 20	320 × 256	15
OP-STIR	142.86	3100/50	90	4	32 × 32	384 × 256	15

are shown in Table 2. This study was approved by the institutional review board, and informed consent was obtained (Ethical Review No. 2014-SR-158). In fact, only bandwidth, matrix and echo train length were adjusted, while the other parameters changed automatically in order to improve image SNR. Then 15 sets of images were graded by two radiologists having experience more than 7 years under double-blind according to a 1–5 scale as follows: grade 1, artifacts obscured the whole plane, grade 2, artifacts obscured both near- and far-field; grade 3, artifacts obscured near-field and the adjacent structures; grade 4, artifacts obscured near-field and did not affect the observation of the adjacent structure; grade 5, no artifacts. Then the image grading difference was analyzed between the same pulse sequence with conventional and optimized parameters [1,18–20].

2.6. Statistical analysis

In this study, to assess the difference of displacement in degrees between titanium alloy and stainless steel materials, Independent-Samples T Test was used. The interreader reliability for image grading was assessed by using Cohen's Kappa statistic [21]. To evaluate the difference of image grading between conventional parameters group and optimized group, Wilcoxon signed-rank test was implemented. All data was processed in SPSS 16.0 Version. Statistical significance was set at $P = 0.05$.

3. Results

The average deflection angles were 4.3° for titanium alloy implants and 7.7° for stainless steel implants. The deflection angle of titanium alloy implants was significantly less than that of stainless steel implants ($t = 9.69$, $P < 0.001$). The test results are shown in Table 3.

The average temperature changes measured by the mercurial thermometer were 0.48 °C for titanium alloy implants and 0.74 °C for stainless steel implants with the background temperature changes of 0.24 °C, which are shown in Table 4. The highest temperature changes for titanium alloy and stainless steel implants were 0.6 °C and 0.9 °C, respectively.

Table 3
Deflection angle of each plate and screw for displacement force test (°).

Number	1	2	3	4	5	6	7
Titanium alloy materials	4.6	3.5	5.4	4.2	4.1	3.8	4.4
Stainless steel materials	9.0	7.5	8.3	7.2	6.9	7.9	7.4

Note. Numbers 1 to 7 represent the implants from left to right in the Picture 1.

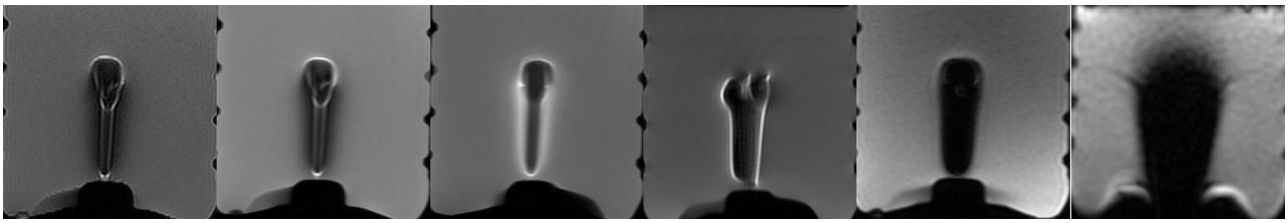

Fig. 6. (a–f):T1-FSE, T2-FSE, STIR, T2-FSE-FS, GRE, DWI. MR images showed artifacts appeared as voids or geometric distortions. Section location oriented to the long axis of the screw and the slice was selected with largest artifacts.

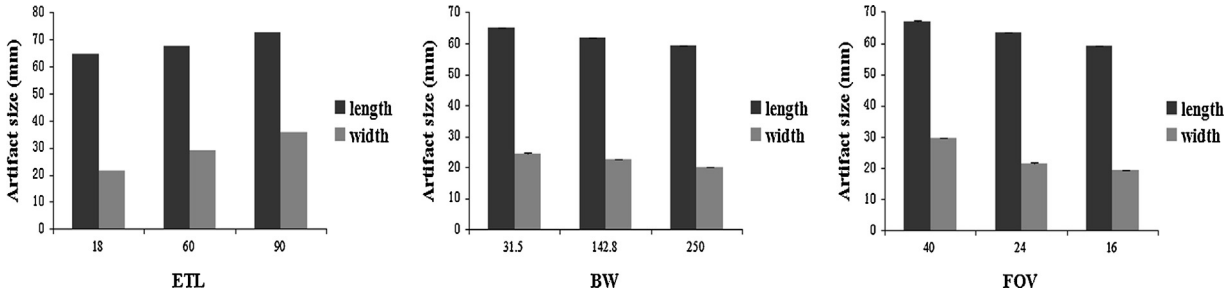

Fig. 7. The histogram showed variation trend of artifacts size by adjusting ETL, bandwidth and FOV, respectively.

Table 4
Temperature changes between pre- and post-MR scan for MRI-related heating test (°C).

Plates	Position	1	2	3	4	5
Titanium alloy	Adjacent to plate	0.4	0.5	0.5	0.4	0.6
materials	Opposite site	0.2	0.2	0.3	0.2	0.3
Stainless steel	Adjacent to plate	0.7	0.7	0.8	0.6	0.9
materials	Opposite site	O.2	0.3	0.3	0.1	0.3

Note. Numbers 1 to 5 represent the implants from left to right in the Picture 3.

Artifact test results are shown in Table 5. The artifacts were appeared as voids or geometric distortions in images shown in Fig. 6. The results revealed diffusion-weighted imaging sequence produced largest artifacts, while fast spin echo pulse sequence produced smallest artifacts. And T2-weighted FSE fat saturation sequence produced larger artifacts than STIR sequence. By altering field of view (FOV), echo train length and bandwidth, respectively, with other parameters keeping unchanged, the variation trend of artifacts size in T2-weighted FSE sequence are shown in Fig. 7. The results showed metallic artifacts increased with longer echo train length and bigger FOV, while decreased with larger bandwidth.

The interreader agreement was good or excellent for each set of image grading. Image quality of sagittal T2-FSE sequence was graded significantly higher for optimized parameters than that with conventional parameters (grade, 3.2 ± 0.4 vs 1.9 ± 0.7, $P = 0.001$; $k = 0.681$ and 0.789). Image grading of axial T2-FSE sequence with optimized parameters was significantly superior to that with conventional parameters (grade, 3.3 ± 0.5 vs 2.7 ± 0.6, $P = 0.003$; $k = 0.837$ and 0.767) and image of STIR sequence received a better grade than that of T2-FSE FS sequence (grade, 3.4 ± 0.5 vs 1.7 ± 0.6, $P < 0.001$; $k = 0.722$ and 0.881) (Fig. 8).

Table 5
Artifacts size of screw in different sequences (mm).

Pulse sequence	Length	Width
FSE-T1	63.6	21.8
FSE-T2	63.0	23.2
STIR	65.8	29.2
FSE-T2-FS	72.0	35.0
GRE	79.5	45.2
DWI	82.2	55.7

Note. The length and width contained the size of screw (length 55 mm, diameter 15 mm).

4. Discussion

4.1. Displacement in degrees

The average deflection angles were 4.3° for titanium alloy implants and 7.7° for stainless steel implants. According to the American Society for Testing and Materials International [10], "if the device deflects less than 45°, then the magnetically induced deflection force is less than the force on the device due to gravity (its weight). For this condition, it is assumed that any risk imposed by the application of the magnetically induced force is not greater than any risk imposed by normal daily activity in the Earth's gravitational field." By comparison, though the deflection angle of stainless steel implants was slightly larger ($t = 41.2$, $P < 0.001$), the magnetically induced force of both kinds of implants was less than their weight, which indicates that it does not pose an additional risk to patients with implants undergoing MRI at 1.5-T or less [7–9]. However, in our study, we did not measure the magnetically induced torque, which cause objects to rotate to align with the magnetic field. ASTM F2213-06 shows the magnetically-induced force and torque are related. If the force is minimal, the torque is expected to minimal as well [9,12].

4.2. MRI-related heating

In this study, MRI-related heating was evaluated on a swine leg fixed with plate by using "worst-case" pulse sequence, which represented the highest specific absorption rate and maximal radio frequency induced heating effect in clinical conditions [9,11,14,15]. The results showed the highest temperature changes were 0.6 °C for titanium alloy implants and 0.9 °C for stainless steel implants. According to Table 4, taking the background temperature changes into consideration the maximum temperature changes contributed by titanium alloy plate was 0.3 °C and 0.6 °C for stainless steel plate. Due to the absence of blood circulation in the swine leg localized heat around the implant cannot be taken away. By this we can deduce that if the implants were in human body, the temperature must have been reduced. Therefore, we can conclude that the minor

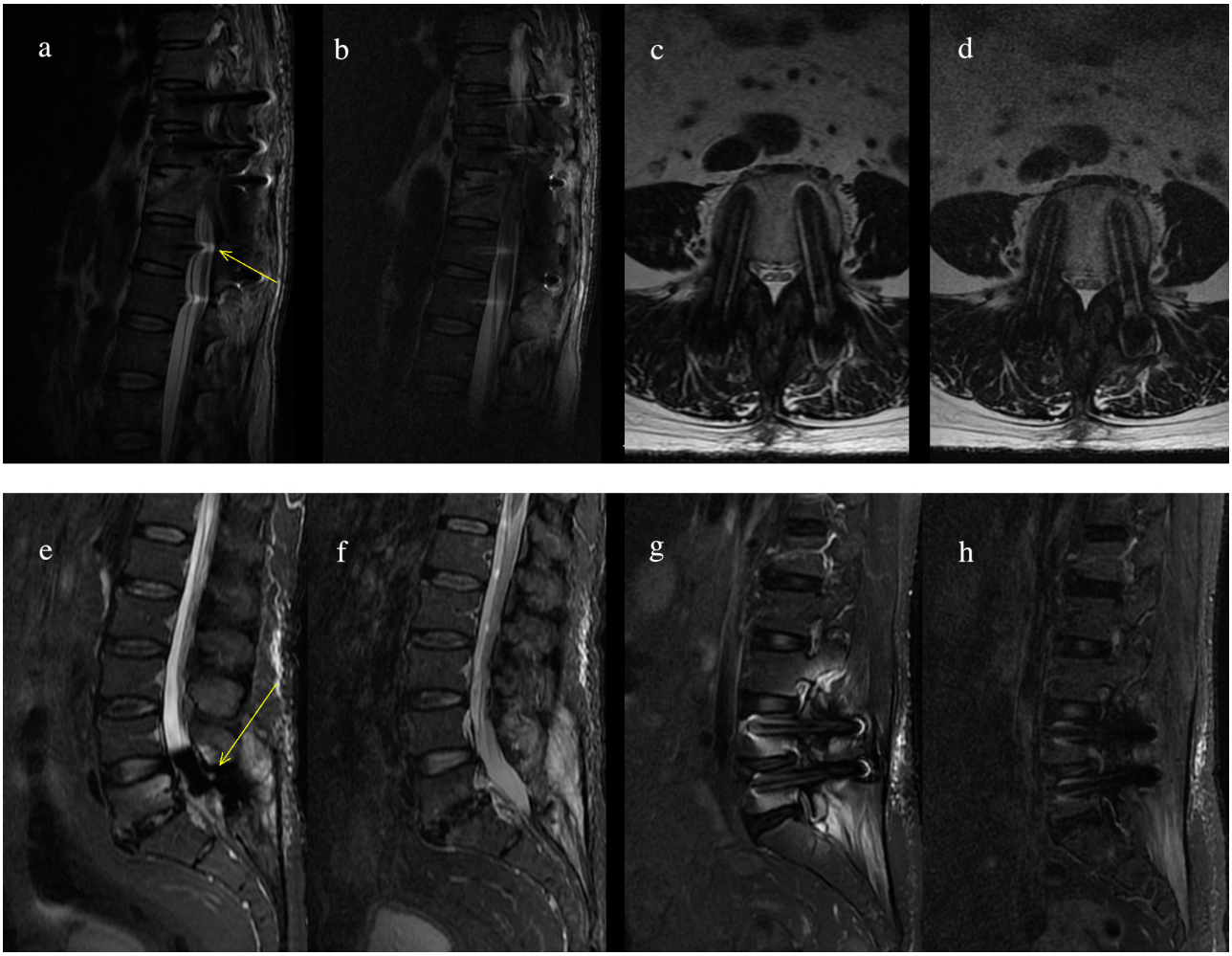

Fig. 8. (a and b) A patient with internal fixation for thoracic vertebral fracture: (a) Sagittal T2-FSE with conventional parameters showing the metallic artifacts obscuring the surrounding structures and the spinal canal geometric distortion (arrow). (b) Sagittal T2-FSE with optimized parameters showing smaller artifacts and the correction of geometric distortion. (c and d) A patient with lumbar fusion for vertebral instability: (d) Axial T2-FSE with optimized parameters show smaller artifacts than (c) the sequence with conventional parameters, while signal-to-noise ratio was a little decreased. (e and f) A patient with lumbar fusion for spondylolysis: (e) T2-FSE fat suppression sequence showing artifacts severely affecting the evaluation of the spinal canal. (f) STIR sequence showing no artifacts on the same slice. (g and h) A patient with lumbar fusion for disc herniation: (g) T2-FSE fat suppression sequence showing geometric distortion and bright pile-up artifacts obscuring the circumferential soft tissue and vertebral body. (h) STIR sequence showing a significant reduction of the artifacts on the same slice. Grades given by the two readers for (a–h) were: 2, 4, 3, 4, 2, 4, 1, 3.

temperature rise caused by both kinds of implants will not produce a thermal injury to a human subject at a 1.5-T MR system or less [8,9,15]. In our heating test, the localized SAR value could be more accurate to reflect the localized condition. As there is no appropriate and practical method to quantify the localized value, the maximal averaged value was used to indicate the "worst-case" condition, which also could represent a worst-case in the localized SAR. It is a limitation in our test.

4.3. Artifacts

Metal implants can cause severe variations in the static magnetic field because of susceptibility variations between metal and surrounding tissue. The inhomogeneous static magnetic field results in substantial image artifacts around implants, including signal loss, failure of fat suppression, geometric distortion, and bright pile-up artifacts [22,23]. Metallic artifacts are primarily associated with magnetic susceptibility, shape and size of the item, as well as parameters used for imaging [1,22,23]. Especially for the orthopedic metal implants mentioned in our study, due to their relatively larger size, we have to consider the impact of artifacts on surrounding soft tissue.

The results of the water phantom study showed image artifacts on T1/T2 weighted FSE sequence were less than GRE sequence, which were agreed on previous reports about inherently larger signal losses in GRE sequence [7–9,15,16]. To avoid signal loss, FSE sequence can offer multiple 180° refocusing pulses that reverses static field dephasing. So it is not difficult to understand the smaller artifacts in FSE sequence. We also found that fat suppression in T2-FSE based on spectrally-selective saturation was failure. Compared with STIR sequence, its artifacts were larger and the figure had geometric distortion. Spectrally-selective saturation FS sequence is more sensitive to inhomogeneous static magnetic field caused by metal, and will fail when chemical shift frequency between fat and water cannot be separated clearly [22]. The best choice of fat suppression was to use STIR imaging because it was completely independent of resonance frequency. STIR uses an inversion recovery approach to suppress fat due to its short T1 relaxation time and then it is able to provide much more homogeneous fat suppression around metal implant [1,22,23]. However, STIR sequence has the low signal-to-noise ratio. And when a contrast agent is used, the contrast-enhanced tissue would instead be suppressed because of its shortened T1. Thus STIR sequence is limited in some cases [22–24]. The results demonstrated that the quality of

diffusion-weighted image was degraded most severely. DWI has additional diffusion gradient field, which can lead to photon dephasing. So it is most sensitive to inhomogeneous static magnetic field because of its effect to aggravate dephasing. Therefore, extensive area around the screw has no signal (Fig. 6). Though artifacts caused by metallic implants could not be ignored, we could choose appropriate sequences to improve image quality, such as FSE and STIR, instead of GRE and spectrally-selective saturation FS sequence [1,15,16,22–24].

In our experiment, we had explored the impact of MR scanning parameters (i.e., FOV, echo train length and bandwidth) on size of metal artifacts. We found metallic artifacts increased with longer echo train length and bigger FOV, while decreased with larger bandwidth. Geometric distortion is inversely proportional to the gradient strength, which scales with bandwidth. So it is able to reduce artifacts by increasing bandwidth and also is a simplest way to reduce metallic artifacts dramatically [1,18,22,23]. We achieved smaller image artifacts by narrowing FOV with matrix unchanged. It meant reducing the voxel size could improve image qualities. Smaller voxels increase the spatial definition of metal-induced signal void and thus reduce apparent size of the void. Furthermore, it helps to reduce diffusion-related signal intensity loss [1,22,23]. However, we found the longer echo train length led to larger artifacts size, which was contrary to previous reports [18,23]. FSE sequence has multiple 180° refocusing pulses and signal intensity of the first echo is strongest, while the remaining becomes weaker and weaker. Therefore, longer echo train length could reduce signal-to-noise ratio (SNR) of image and also degrades the quality of image with metal, seemingly like to larger artifacts in our measurements. Thus appropriate echo train length should be selected to reduce artifacts and prevent the decrease of signal-to-noise ratio. Taking above mentioned into consideration, we had performed parameters modification and optimization on pulse sequences of axial T2-FSE, sagittal T2-FSE and STIR. 15 volunteers with internal vertebral fixation (titanium alloy materials) were both performed MR scan with conventional and optimized parameters. And all images acquired were graded by two radiologists having the experience of more than 7 years, images of sagittal T2-FSE sequence were graded significantly higher for optimized parameters than that with conventional parameters (grade, 3.2 ± 0.4 vs 1.9 ± 0.7, $P = 0.001$). Image grading of axial T2-FSE sequence with optimized parameters was significantly superior to that with conventional parameters (grade, 3.3 ± 0.5 vs 2.7 ± 0.6, $P = 0.003$) and image of STIR sequence received a better grade than that of T2-FSE FS sequence (grade, 3.4 ± 0.5 vs 1.7 ± 0.6, $P < 0.001$) (Fig. 8). It was obvious that metallic artifacts had been significantly reduced by optimized parameters, though SNR of image decreased to a certain extent. Therefore, pulse sequences with optimized parameters showed in Table 2 have a big advantage on displaying localized complications of passive implants, especially for patients with clinical symptoms but normal or equivocal on X-ray plain film [1,18,22–25].

5. Conclusions

Our study was performed to evaluate MR issues for the latest standard brands of plates and screws used in orthopedic surgery at a 1.5-T MR system, including displacement in degrees, MRI-related heating, and artifacts. The results indicate that both titanium alloy and stainless steel materials (plates and screws) cause a weak force and low MRI-related heating at a 1.5-T or less, which do not pose an additional hazard or risk to patients. However, metallic artifacts should not be ignored because of their relative larger size, especially when region of interest is adjacent to implants. And it is possible to minimize artifacts by choosing appropriate pulse sequences and optimizing scanning parameters, such as FSE and STIR sequence with large bandwidth, small FOV and appropriate echo train length.

Conflicts of interest

All authors declare no conflicts of interest.

Acknowledgments

We thank the department of Spine Surgery, Bone and Joint Surgery for providing titanium alloy and stainless steel plates and screws conforming to the latest standard brands.

Appendix A. Supplementary data

Supplementary data associated with this article can be found, in the online version, at http://dx.doi.org/10.1016/j.ejrad.2014.12.001.

References

[1] White LM, Kim JK, Mehta M, et al. Complications of total hip arthroplasty: MR imaging−−initial experience 1. Radiology 2000;215(1):254–62.
[2] Young PM, Berquist TH, Bancroft LW, et al. Complications of spinal instrumentation. RadioGraphics 2007;27:775–89.
[3] Chang EY, McAnally JL, Van Horne JR, et al. Metal-on-metal total hip arthroplasty: do symptoms correlate with MR imaging findings? Radiology 2012;265(3):848–57.
[4] Sofka CM, Potter HG, Adler RS, et al. Musculoskeletal imaging update: current applications of advanced imaging techniques to evaluate the early and long-term complications of patients with orthopedic implants. HSS J 2006;2(1):73–7.
[5] Weiland DE, Walde TA, Leung SB, et al. Magnetic resonance imaging in the evaluation of periprosthetic acetabular osteolysis: a cadaveric study. J Orthop Res 2005;23(4):713–9.
[6] Walde TA, Weiland DE, Leung SB, et al. Comparison of CT, MRI, and radiographs in assessing pelvic osteolysis: a cadaveric study. Clin Orthop Relat Res 2005;437:138–44.
[7] Gill A, Shellock FG. Assessment of MRI issues at 3-Tesla for metallic surgical implants: findings applied to 61 additional skin closure staples and vessel ligation clips. J Cardiovasc Magn Reson 2012;14:3.
[8] Audet-Griffin AJ, Pakbaz S, Shellock FG. Evaluation of MR safety for a new liquid embolic device. J Neurointerv Surg 2013;6(8):624–9 (neurintsurg-2013-010877).
[9] Yang C, Liu L, Wang J, et al. Magnetic resonance imaging of artificial lumbar disks: safety and metal artifacts. Chin Med J (Engl Ed) 2009;122(8):911–6.
[10] American Society for Testing and Materials International. F2052. Standard test method for measurement of magnetically induced displacement force on passive implants in the magnetic resonance environment. In: Annual book of ASTM standards: medical devices. Volume 13.01. West Conshohocken, PA: American Society for Testing and Materials; 2002. p. 1576–80.
[11] Shellock FG, Valencerina S. In vitro evaluation of MR imaging issues at 3 T for aneurysm clips made from MP35N: findings and information applied to 155 additional aneurysm clips. Am J Neuroradiol 2010;31(4):615–9.
[12] American Society for Testing and Materials International. Designation F2213-06: standard test method for measurement of magnetically induced torque on medical devices in the magnetic resonance environment. West Conshohocken, PA: ASTM International; 2006.
[13] Karacozoff AM, Shellock FG, Wakhloo AK. A next-generation, flow-diverting implant used to treat brain aneurysms: in vitro evaluation of magnetic field interactions, heating and artifacts at 3-T. Magn Reson Imaging 2013;31(1):145–9.
[14] American Society for Testing and Materials International. Designation F 2182-011a. Standard test method for measurement of radio frequency induced heating near passive implants during magnetic resonance imaging. West Conshohocken, PA: ASTM International; 2011.
[15] Shellock FG, Knebel J, Prat AD. Evaluation of MRI issues for a new neurological implant: the Sensor Reservoir. Magn Reson Imaging 2013;31(7):1245–50.
[16] Dedini RD, Karacozoff AM, Shellock FG, et al. MRI issues for ballistic objects: information obtained at 1.5-: 3-and 7-Tesla. Spine J 2013;13(7):815–22.
[17] American Society for Testing and Materials International. F2119-01 A. Standard test method for evaluation of MR image artifacts from passive implants. West Conshohocken, PA: ASTM International; 2001.
[18] Cha JG, Hong HS, Park JS, et al. Practical application of iterative decomposition of water and fat with echo asymmetry and least-squares estimation (IDEAL) imaging in minimizing metallic artifacts. Korean J Radiol 2012;13(3):332–41.
[19] Chen CA, Chen W, Goodman SB, et al. New MR imaging methods for metallic implants in the knee: artifact correction and clinical impact. J Magn Reson Imaging 2011;33(5):1121–7.

[20] Sasaki T, Hansford R, Zviman MM, et al. Quantitative assessment of artifacts on cardiac magnetic resonance imaging of patients with pacemakers and implantable cardioverter-defibrillators. Circ: Cardiovasc Imaging 2011;4(6):662–70.
[21] Navalho M, Resende C, Rodrigues AM, et al. Bilateral MR imaging of the hand and wrist in early and very early inflammatory arthritis: tenosynovitis is associated with progression to rheumatoid arthritis. Radiology 2012;264(Sep (3)):823–33.
[22] Hargreaves BA, Worters PW, Pauly KB, et al. Metal-induced artifacts in MRI. Am J Roentgenol 2011;197(3):547–55.
[23] Lee MJ, Kim S, Lee SA, et al. Overcoming artifacts from metallic orthopedic implants at high-field-strength MR imaging and multi-detector CT1. Radiographics 2007;27(3):791–803.
[24] Sutter R, Ulbrich EJ, Jellus V, et al. Reduction of metal artifacts in patients with total hip arthroplasty with slice-encoding metal artifact correction and view-angle tilting MR imaging. Radiology 2012;265(1):204–14.
[25] Cha JG, Jin W, Lee MH, et al. Reducing metallic artifacts in postoperative spinal imaging: usefulness of IDEAL contrast-enhanced T1- and T2-weighted MR imaging––phantom and clinical studies. Radiology 2011;259(3):885–93.